RAMMS::EXTENDED – SENSITIVITY ANALYSIS OF NUMERICAL FLUIDIZED POWDER AVALANCHE SIMULATION IN THREE-DIMENSIONAL TERRAIN

J. Glaus [1,2,4] *, K. Wikstrom Jones[3], Y. Bühler[1,2], M. Christen [1,2], P. Ruttner-Jansen [1,2,5], J. Gaume [1,2,4] and P. Bartelt [1,2]

[1] *WSL Institute for Snow and Avalanche Research SLF, Davos Dorf, Switzerland*
[2] *Climate Change, Extremes, and Natural Hazards in Alpine Regions Research Center CERC, Davos Dorf, Switzerland*
[3] *Alaska Division of Geological & Geophysical Surveys, Anchorage, AK, USA*
[4] *Institute for Geotechnical Engineering, ETH Zürich, Switzerland*
[5] *Institute of Geodesy and Photogrammetry, ETH Zürich, Zurich, Switzerland*

ABSTRACT: In this paper, we present a sensitivity analysis of RAMMS::EXTENDED, a numerical software for avalanche simulations that includes the reconstruction of the avalanche core and powder cloud. It is a further developed version of the well known avalanche simulation tool RAMMS::AVALANCHE. Our results are based on the reconstruction of an avalanche that released in 2019 in the Dischma Valley, Switzerland. The avalanche was surveyed with drone-based photogrammetry and provides detailed information about the expansion of the release zone, snow height and avalanche run-out. First, the analysis is carried out on a planar surface representing the avalanche track, and excludes the effects of the terrain. In a second step, the same parameters are tested on a digital terrain model that represents the real avalanche path. Both topographies are evaluated for a local and a global sensitivity analysis. The analysis is restricted on the input parameters a practitioner can measure, the disposition of mass on the slope (release depth, erosion depth and erosion gradient) and the snow temperature (release temperature and snowpack temperature gradient) were varied. The result of the analysis helps to better understand the influence of each model parameter.
KEYWORDS: avalanche simulation, powder avalanche, entrainment, road safety

1. INTRODUCTION

The **RAMMS::AVALANCHE** model has relied on empirical, calibrated friction parameters of the Voellmy-type (Voellmy, 1955) to simulate avalanche run-out in three-dimensional terrain (Christen et al., 2010). These parameters can be adjusted to account for climate and elevation (Ortner et al., 2023) allowing the application of the model in different mountain environments. This procedure has been well-received by the snow avalanche mitigation community and **RAMMS::AVALANCHE** remains a popular simulation tool. However, the model cannot address increasingly important problems arising from practice, or, problems associated with changing climate. In particular, snow entrainment, different avalanche flow regimes (wet avalanches or impact pressures arising from the powder cloud) cannot be simulated. Presently, forest interaction is included in the **RAMMS::AVALANCHE** model by adjusting friction parameters Vedrine et al., 2022 and Feistl, 2015.

To address these problems the Institute for Snow and Avalanche Research (SLF) has ”extended” the existing **RAMMS::AVALANCHE** model to include many additional physical processes, including snow entrainment, a more advanced forest interaction model, powder cloud formation and turbulence as well as avalanche flow regime transitions, typically controlled by snow temperature and moisture content. Similar to the **RAMMS::AVALANCHE** model, the extended model has been designed around existing Swiss guideline procedures to facilitate use by practitioners (Salm et al., 1990). The model retains the depth-averaged framework (i.e. no additional computer resources are required) and therefore can be applied to simulate avalanches at the regional, or even country scale (Ortner et al., 2023). Although the **RAMMS::EXTENDED** model is certainly more complex, the graphical-user interface has likewise been developed to visualize mass balance, temperature, forest destruction, and, perhaps most importantly, powder cloud impact pressures.

The purpose of this paper is to demonstrate how avalanche scenarios modeled in **RAMMS::EXTENDED** react to changing initial and boundary conditions, most notably to release and entrainment variables such as snow temperature and elevation effects which are introduced into the model by specifying height/temperature gradients of the mountain snowcover. To a large extent, these parameters drive avalanche flow regime transitions, and therefore the formation of powder avalanches, or the transition to dense, wet avalanches. They are essential for climate change impact studies (Ortner et al., 2023). To use the **RAMMS::EXTENDED** model, users will require

*Corresponding author address:
Julia Glaus, WSL Institute for Snow and Avalanche Research SLF, 7276 Davos Dorf, Switzerland;
tel: +41 78 633 44 05
email: julia.glaus@slf.ch

some guidelines and knowledge on the handling of the newly introduced parameters. Moreover, the increasing complexity of the **RAMMS::EXTENDED** model also has severe drawbacks from the practical standpoint as it demands information that is often unknown and unfamiliar. In the future, as all avalanche models become more complex, more model set-up information and understanding of the effect of each model parameter will be required. To demonstrate the importance of this problem we will perform a sensitivity analysis on two avalanche tracks: an idealized slope and an established avalanche path in the Dischma valley, located near Davos, Switzerland. We begin, however, with a mathematical overview of the **RAMMS::EXTENDED** model.

2. METHODS

2.1 Model Equations

Depth-averaged models to simulate mixed flowing/powder snow avalanches were first proposed by Russian researchers in the late 1980s (Nazarov, 1991; Bozhinskiy et al., 1998). Since then, many mathematical models have been developed to describe powder snow avalanches such as Issler, 1998, Naaim et al., 1998 and Turnbull et al., 2007. The Russian researchers divided the avalanche into two layers, which we designate the avalanche core Φ and powder cloud Π, see Figure 1.

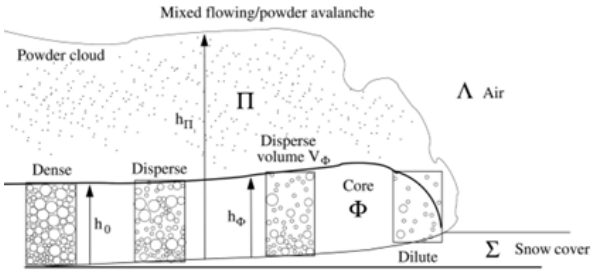

Figure 1: The mixed flowing/powder avalanche is split into two layers, the core Φ and cloud Π. The core and cloud interact with the snowcover Σ and surrounding air Λ (Bartelt et al., 2015a).

The core layer Φ consists of interacting lumps and clods of snow (particles) and is modelled as granular shear flow; the cloud consists of ice-dust and air and is modelled as a turbulent, suspension flow. The avalanche core interacts with the snowcover, which we treat as an erodible substrate (designated Σ). Turbulent structures in the cloud serve to entrain the surrounding air (designated Λ).

The avalanche core Φ travels with the mean velocity $\vec{u}_\Phi$; the ice dust mixture in the powder cloud travels with the mean powder velocity $\vec{u}_\Pi$. The velocity vectors ($\vec{u}_\Phi$,$\vec{u}_\Pi$) are defined in the slope-parallel directions. Depth-averaged mass balance equations for the core Φ are

$$\partial_t \hat{h}_\Phi + \boldsymbol{\nabla} \cdot (\hat{h}_\Phi \vec{u}_\Phi) = \frac{\rho_\Sigma}{\hat{\rho}_\Phi} \dot{M}_{\Sigma\to\Phi} - \dot{M}_{\Phi\to\Psi} - \frac{\hat{\rho}_\Pi}{\hat{\rho}_\Phi} \dot{M}_{\Phi\to\Pi} \tag{1}$$

$$\partial_t h_\Phi + \boldsymbol{\nabla} \cdot (h_\Phi \vec{u}_\Phi) = \mathbb{D}(t) \tag{2}$$

and for the powder cloud Π:

$$\partial_t \hat{h}_\Pi + \boldsymbol{\nabla} \cdot (\hat{h}_\Pi \vec{u}_\Pi) = \dot{M}_{\Phi\to\Pi} \tag{3}$$

$$\partial_t h_\Pi + \boldsymbol{\nabla} \cdot (h_\Pi \vec{u}_\Pi) = \dot{M}_{\Lambda\to\Pi} + \nu_\Lambda \dot{M}_{\Phi\to\Pi}. \tag{4}$$

where $\boldsymbol{\nabla}$ is the divergence operator in Cartesian coordinates. Each pair of differential equations for the core and cloud (Φ, Π) is written for the co-volume heights ($\hat{h}_\Phi$, $\hat{h}_\Pi$) with densities ($\hat{\rho}_\Phi$,$\hat{\rho}_\Pi$) and for the real avalanche flow heights (h_Φ, h_Π) with densities (ρ_Φ,ρ_Π).

The mass balance equations contain entrainment and mass exchange rates with dimension of velocity (m/s) which are denoted by the symbol $\dot{M}$. The term $\dot{M}_{\Sigma\to\Phi}$ defines the rate at which snow of density ρ_Σ is being entrained by the avalanche. Entrainment is parameterized by a single dimensionless parameter (Bartelt et al., 2018), the snow erodibility κ_Σ, with,

$$\dot{M}_{\Sigma\to\Phi} = \kappa_\Sigma ||\vec{u}_\Phi||. \tag{5}$$

The term $\dot{M}_{\Lambda\to\Pi}$ defines the air (density ρ_Λ) entrainment rate into the powder cloud. The term $\dot{M}_{\Phi\to\Pi}$ quantifies the transfer of dust from the avalanche core Φ to the cloud Π (ν_Λ is the volumetric fraction of air of the mass exchange). The snow mass stopped by a forest is denoted $\dot{M}_{\Phi\to\Psi}$ (Feistl, 2015).

We describe dispersing processes by a differential inclusion $\mathbb{D}(t)$, which we regard to be a highly dynamic function, varying in both space and time. The inclusion $\mathbb{D}(t)$ describes the change in the avalanche core height by dispersive pressures, which lead to both fluidization and the intake of air; resulting in the formation of the powder cloud. It accounts for sudden changes in shear rate and the collisional interaction with the snowcover which lead to a dynamic expansion (dilatancy) of the granular core (see Buser et al., 2009 for more details).

We have momentum conservation equations for the core,

$$\begin{aligned} &\partial_t(\hat{h}_\Phi \vec{u}_\Phi) + \boldsymbol{\nabla} \cdot \left(\hat{h}_\Phi \vec{u}_\Phi \otimes \vec{u}_\Phi + p_\Phi I\right) = \\ &\vec{G}\hat{h}_\Phi - \frac{\vec{u}_\Phi}{||\vec{u}_\Phi||}\boldsymbol{S}_\Phi - \left[\dot{M}_{\Phi\to\Pi} + \frac{\hat{\rho}_\Pi}{\hat{\rho}_\Phi}\dot{M}_{\Phi\to\Pi}\right]\vec{u}_\Phi \end{aligned} \tag{6}$$

and the cloud,

$$\begin{aligned} &\partial_t(\hat{h}_\Pi \vec{u}_\Pi) + \boldsymbol{\nabla} \cdot \left(\hat{h}_\Pi \vec{u}_\Pi \otimes \vec{u}_\Pi + p_\Pi I\right) = \\ &\left[\frac{\hat{\rho}_\Pi - \rho_\Lambda}{\hat{\rho}_\Pi}\right]\vec{G}\hat{h}_\Pi + \dot{M}_{\Phi\to\Pi}\vec{u}_\Pi \\ &- \frac{\vec{u}_\Pi}{||\vec{u}_\Pi||}\boldsymbol{S}_\Pi - \frac{\rho_\Lambda}{\hat{\rho}_\Pi}\dot{M}_{\Lambda\to\Pi}\vec{u}_\Pi. \end{aligned} \tag{7}$$

The symbol $\otimes$ denotes the tensor product and I is the two dimensional unity matrices. The right-hand side includes the driving force of gravity $\vec{G} = (g_x, g_y)$ which is balanced by frictional (shear) resistance, (S_Φ, S_Π). In the powder equation we pre-multiply the driving gravitational force with the density difference between the dust $\hat{\rho}_\Pi$ and the air ρ_Λ to take into account buoyancy. The powder cloud equation includes an additional driving force – the momentum transferred with the mass exchange between the core and the cloud $\dot{M}_{\Phi\to\Pi}$. The pressures (p_Φ, p_Π) include the hydrostatic pressure of the flow, including centrifugal (terrain curvature) and dispersive accelerations (Bartelt et al., 2015b).

To parameterize friction (S_Φ, S_Π) in the avalanche core Φ and cloud Π we introduce two additional state variables in the model. Both variables describe the kinetic energy associated with three-dimensional velocity fluctuations ($\vec{u}'_\Phi$, $\vec{u}'_\Pi$) in the core $\tilde{u}_\Phi = \vec{u}_\Phi + \vec{u}'_\Phi$ and cloud $\tilde{u}_\Pi = \vec{u}_\Pi + \vec{u}'_\Pi$, respectively,

$$R_\Phi = \frac{\hat{\rho}_\Phi}{2}||\vec{u}'_\Phi||^2 \qquad R_\Pi = \frac{\hat{\rho}_\Pi}{2}||\vec{u}'_\Pi||^2. \tag{8}$$

The state variable R_Φ, the so-called *granular temperature* or *random kinetic energy*, is utilized to describe the dispersion of the granular snow and therefore facilitates the formulation of constitutive models including the effects of variable flow density and particle interactions in the avalanche core Φ (Buser et al., 2009). The state variable R_Π is a measure of the turbulence within the powder cloud and facilitates not only formulation of cloud drag models, but also the turbulent entrainment of air, and subsequently the dispersion of dust, the height of the cloud as well as the intensity of the impact pressures (Zhuang et al., 2023). Random energy fluxes of (R_Φ,R_Π) are governed by two production/decay equations for the core,

$$\begin{aligned}&\partial_t(\hat{h}_\Phi R_\Phi) + \boldsymbol{\nabla}\cdot(\hat{h}_\Phi R_\Phi \vec{u}_\Phi) = \\ &\alpha_\Phi \dot{W}_\Phi - \dot{M}_{\Phi\to\Pi} R_\Phi - \beta_\Phi \hat{h}_\Phi R_\Phi + \epsilon_\Phi \rho_\Sigma \dot{L}_{\Sigma\to\Phi}\end{aligned} \tag{9}$$

and the cloud

$$\begin{aligned}&\partial_t(\hat{h}_\Pi R_\Pi) + \boldsymbol{\nabla}\cdot(\hat{h}_\Pi R_\Pi \vec{u}_\Pi) = \\ &\dot{W}_\Pi + \dot{M}_{\Phi\to\Pi} R_\Phi + \frac{1}{2}\rho_\Lambda \dot{M}_{\Lambda\to\Pi}||\vec{u}_\Pi||^2 - \beta_\Pi \hat{h}_\Pi R_\Pi.\end{aligned} \tag{10}$$

In both cases, the primary source of the velocity fluctuations is shearing, $\dot{W}_\Phi = \hat{\rho}_\Phi \boldsymbol{S}_\Phi ||\vec{u}_\Phi||$ and $\dot{W}_\Pi = \hat{\rho}_\Pi \boldsymbol{S}_\Pi ||\vec{u}_\Pi||$. In the case of the core, only the $\alpha_\Phi < 1$ part of the shear work $\dot{W}_\Phi$ is converted to random kinetic energy (the remaining part is dissipated immediately to heat). The parameter α_Φ is a temperature dependent parameter, with higher values associated with colder snow. An important source of random kinetic energy is snow entrainment, which is treated as a fully plastic collision between the avalanche and the erodible snowcover (Bartelt et al., 2018). During this process, which demands the break-up, compaction and rearrangement of the entrained snow, energy is dissipated at the rate $\dot{L}_{\Sigma\to\Phi} = \frac{1}{2}\dot{M}_{\Sigma\to\Phi}||\vec{u}_\Phi||^2$. The ϵ_Φ-th fraction of this energy is transformed to macroscopic random energy, before being dissipated to heat.

In the case of the cloud, the entire shear work $\dot{W}_\Pi$ is converted to turbulence. Random energies in the core and powder cloud both dissipate to heat at the rates (β_Φ, β_Π). These decay coefficients determine the longevity of the random and turbulent kinetic energies in the core and powder cloud. In the core, the parameter β_Φ increases with temperature and moisture content. In the cloud, there are two additional sources of turbulence: the entrainment of air $\dot{M}_{\Lambda\to\Pi}$, primarily at the outer surface of the cloud, as well the transfer of random kinetic energy R_Φ with the dust mass that is blown-out of the core $\dot{M}_{\Phi\to\Pi}$ in the formation phase. Thus, when core mass is transferred to the cloud, the associated momentum, as well as turbulent and internal energies are likewise transported to the cloud.

The **RAMMS::EXTENDED** model predicts the mean avalanche temperature T_Φ with a balance equation that tracks the internal energy $E_\Phi = \hat{\rho}_\Phi c_\Phi T_\Phi$ of the avalanche core, where c_Φ is the specific heat capacity of snow at the density ρ_Φ. The balance equation contains *seven* source terms on the right-hand side,

$$\begin{aligned}&\partial_t(\hat{h}_\Phi E_\Phi) + \boldsymbol{\nabla}\cdot(\hat{h}_\Phi E_\Phi \vec{u}_\Phi) = \\ &(1-\alpha_\Phi)\,\dot{W}_\Phi - \dot{M}_{\Phi\to\Pi} E_\Phi + \beta_\Phi \hat{h}_\Phi R_\Phi \\ &(1-\epsilon_\Phi)\,\rho_\Sigma \dot{L}_{\Sigma\to\Phi} + \rho_\Sigma c_\Sigma T_\Sigma \dot{M}_{\Sigma\to\Phi} - \dot{Q}_m - \dot{q}_{\Phi\to\Lambda}\end{aligned} \tag{11}$$

The term $\dot{Q}_m$ represents the latent heat of melting ice,

$$\int_0^{\Delta t} \dot{Q}_m dt = \rho_i c_i \hat{h}_i \left[T_i - T_m\right]. \tag{12}$$

The constant T_m is the melting temperature of ice. The associated change in mass is $\dot{Q}_m/L$ where L is the latent heat of ice. The remaining terms on the right-hand side account for the addition of heat energy from entrained snow and the fraction of heat energy produced during the plastic collision of the snowcover and finally the sensible heat exchange ($q_{\Phi\to\Lambda}$) of the flowing snow with the air. An additional mass balance equation accounts for the intake of bonded water in the snowcover and melting (Valero et al., 2017)

$$\partial_t \hat{h}_w + \boldsymbol{\nabla}\cdot(\hat{h}_w \vec{u}_\Phi) = \frac{\rho_\Sigma}{\rho_w}\eta_w \dot{M}_{\Sigma\to\Phi} + \frac{\dot{Q}_m}{\rho_w L}. \tag{13}$$

The parameter η_w defines the volumetric water fraction in the entrained snow.

2.2 Frictional Resistance

Frictional resistance in the avalanche core Φ is described by a dilatant and water-dependent Voellmy-

type friction law,

$$S_\Phi = \mu_\Phi N_\Phi + (1-\mu_\Phi) N_0 \left[1 - \exp\left(-\frac{N_\Phi}{N_0}\right)\right] + \rho_\Phi g \frac{||\vec{u}_\Phi||^2}{\xi_\Phi} \quad (14)$$

Experiments with granular materials (Liu et al., 2021) and snow (Bartelt et al., 2015a) indicate a non-linear relationship between the shear stress S_Φ and normal force N_Φ. Measurements indicate a sharper increase in shear S_Φ at relatively low normal stresses (small flow heights). The value of N_0 defines the normal stress at which the non-linearity occurs, shifting the shear stress upwards to account for cohesive bonding and/or locking between the granules.

The friction law is formulated by first defining the base-friction in the mixture co-volume (μ_{Φ_0}, ξ_{Φ_0}). We account for the presence of water in the mixture by adjusting the value of the Coulomb friction according to,

$$\mu_{\Phi_{wet}} = \mu_{wet} + (\mu_{\Phi_0} - \mu_{wet}) \exp\left(-\frac{\hat{h}_w}{h_{w0}}\right) \quad (15)$$

where μ_{wet} defines the friction of a fully saturated mixture. The Coulomb friction decreases from μ_{Φ_0} to μ_{wet} according to an exponential law governed by the parameter h_{w0}, the so-called dry-wet transition parameter. Small values of h_{w0} are associated with the existence of small water films on the granular material that leads to an immediate reduction in the Coulomb friction. High values of h_{w0} appear to represent the concentration of water near the basal running surface of the avalanche. In this case, a part of the flow material remains dry and non-lubricated. The model formulation clearly does not account for the spatial distribution of water in the granular mixture, and represents a major limitation of depth-averaged approaches. We follow the work of Valero et al., 2017 and take h_{w0}=100mm with μ_{wet}=0.12. A similar procedure is applied to define the influence of water on the velocity-squared drag,

$$\xi_{\Phi_{wet}} = \xi_{wet} + (\xi_{\Phi_0} - \xi_{wet}) \exp\left(-\frac{\hat{h}_w}{h_{w0}}\right). \quad (16)$$

In this case the ξ_{Φ_0} is reduced. Because ξ_{Φ_0} enters the Voellmy-formulation as an inverted function, this implies that the velocity-squared friction is increased. This formulation enables wet snow avalanches to flow over low angle terrain with a much lower velocity than dry snow avalanches. The decrease in ξ_{Φ_0} can thus be interpreted as an increase in the effective viscosity of the material with an increase of water content. At the present stage of the constitutive development for S_Φ we have not considered a modification of the flow friction due to changes in flow density. While flowing, however, the flow dilates, leading to a dispersion of the granular ensemble. As a result, the effective friction of the mixture decreases. We term this process granular fluidization. We account for this difference with the concept of activation energy A_Φ. The activation energy quantifies the shear work necessary to fluidize the solid material of the flowing avalanche. The activation energy is then utilized in an exponential law to reduce the co-volume based, lubricated friction values,

$$\mu_\Phi = \mu_{\Phi_{wet}} \exp\left[\frac{-R_\Phi^D}{A_\Phi}\right], \frac{1}{\xi_\Phi} = \frac{1}{\xi_{\Phi_{wet}}} \exp\left[\frac{-R_\Phi^D}{A_\Phi}\right]. \quad (17)$$

The value R_Φ^D is the fraction of the granular fluctuations which induces a change in volume in the granular ensemble. For example, if we assume that the fluctuation energy R_Φ in the core Φ is distributed evenly in all three coordinate directions we would have one-third of the of energy in the slope-perpendicular z-direction.

As for the powder cloud, the total drag resistance is composed of a laminar and a turbulent component, and can be written as:

$$S_\Pi = \hat{\rho}_\Pi \left[\mu_L ||\vec{u}_\Pi|| + \mu_T R_\Pi \hat{h}_\Pi\right] \quad (18)$$

μ_L and μ_T are sets of laminar/turbulent parameters controlling the cloud drag. They are defined by back-calculations of recorded real avalanche events. In the drag relationship, the first term $\mu_L \vec{u}_\Pi$ represents the laminar drag and is the function of the average velocity $\vec{u}_\Pi$. The second term $\mu_T R_\Pi \hat{h}_\Pi$ represents the turbulent resistance and is a function of the turbulent energy of the powder cloud R_Π, which implies the contribution of the velocity fluctuation. Higher velocities are associated with large turbulent drag. At lower velocities the turbulence has dissipated and the flow is laminar.

2.3 Model Setup and Data

We conduct a single-track sensitivity study by varying input parameters which the user can directly measure in the field (as shown in Table 1). In the study, we varied the parameters one-at-a-time and using an interval of realistic values representing with the minimum/maximum values also extreme scenarios (Saltelli et al., 2000). The range of values agree with measurements from Intercantonal Measuring and Information System (IMIS) weather stations. In the sensitivity analysis, we focus on avalanche inundation area, studying both avalanche flow width and run-out distance. We concentrate on a well documented event at Ruechi Tobel as this allows a comparison between return period and three-day new snow heights (see Figure 2). Some mechanical parameters which are set as constant for the user in **RAMMS::EXTENDED** as snow density and friction were chosen by back-calculation.

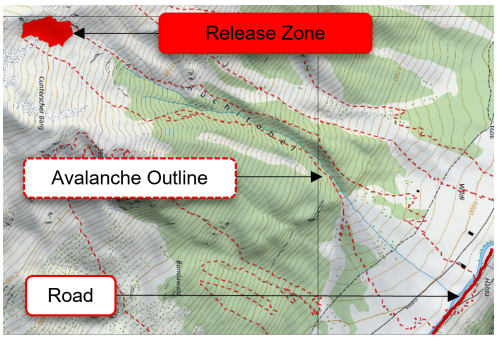

Figure 2: Depiction of the Ruechi Tobel release zone and measured outline of the 16.01.2019 avalanche. The artificially released avalanche crossed the road.

Snow cover disposition	Value
Release height d_0	0.9 m
Release density ρ_0	200 kg/m^3
Erosion height d_0^*	1.05 m
Erosion gradient ΔD	0.03 m/100m
Erosion density ρ_Σ	200 kg/m^3
Release temperature T	-6 ℃
Temperature gradient ΔT	0.3 °C/100m

Table 1: Snow height and temperature disposition.

In the analysis, two groups of sensitivity parameters are defined. The first group describes the disposition of mass on the slope and includes release depth d_0, erosion depth d_0^* and snow cover depth gradient ΔD from release to run-out. The release depth is the average three-day snow height in the slope-perpendicular direction. The depth d_0^* defines the maximum potential erosion depth. The snowcover gradient refers to the decrease in snow depth per 100 m drop in altitude, which is also adjusted according the slope angle in accordance with the Swiss calculation guidelines (Salm et al., 1990). The second group of parameters in the sensitivity analysis represent the influence of snow temperature on the run-out: the average snow temperature T of the snow in the release zone and the temperature gradient ΔT which describes the temperature increase for every 100 m drop in altitude.

In the sensitivity analysis, we did not vary the areal extent and location of the release zone (only the release depth). Instead, we used the release zone of an artificially triggered powder-snow avalanche in the Ruechi Tobel avalanche path observed on January 16th, 2019 . This case provides excellent data about the release zone dimension (the stauchwall, the lower bound of the release zone, was clearly visible). The release zone has a measured area of 9000 m^2. This data was collected by structure-from-motion photogrammetry from a drone. Snow heights were derived by subtracting the post-avalanche elevation surface from the bare ground (summer) surface. Air and snow temperature data was collected from nearby weather stations (e.g. the IMIS Stations SLF2 and Stillberg), and was used to set initial model parameter values. Additionally, video footage provided qualitative insights into the cloud height and velocity. This procedure allows us to include an actual event in our sensitivity analysis, serving to anchor the analysis to a concrete event. We performed the sensitivity analysis by varying parameters values near the values obtained based on the back-calculated real event. Moreover, the calculated avalanche run-out, flow width and powder cloud height of the simulated avalanches were near the observed values of the January 16th, 2019, avalanche. Parameter values for the case study are reported in Table 1.

In a first step, we simulated the avalanche on a simplified planar slope which has roughly the steepness of the Ruechi Tobel avalanche path and with identifiable release volume (see Figure 3). In this step, we investigated the influence of the parameter variations without three-dimensional terrain effects. In a second step, the same simulations are calculated on a (summer) DEM including realistic terrain effects.

We measured the travel length of the avalanche by measuring the distance between the uppermost point of the release zone to the outermost point in the run-out zone. We evaluated the maximum values of the core velocity and powder pressure over this distance. The outlines represent the avalanche deposits and are defined by the points where the avalanche core is higher than 0.1 m and its velocity lower than 1 m/s. For the powder cloud, the outline is defined by a threshold value of 0.5 kPa. We simulated the avalanche using a grid resolution of 5 m.

3. RESULTS AND DISCUSSION

The results of the sensitivity analysis are depicted in the overview Figure 4. The first column presents numerical graphs plotting the run-out distance of the avalanche core Φ and powder cloud Π as a function of the two parameter sets. The remaining columns in the graph show the calculated outlines of the core and cloud on both the real (columns 2 and 3) and idealized slope (columns 4 and 5). In general, the shape of the cloud is strongly influenced by the shape of the core as all the mass of the cloud evolves from the core. The comparison of the idealised slope and the summer DEM shows similar trends when varying input parameters with longer run-out distances for the idealised slope due to reduced surface roughness. On the planar slope the avalanche will pile up snow at the beginning of the flat run-out, and extends from there in length and width based on a unique combination of released and entrained snow mass and temperature. This strongly influences the shape and length of the avalanche. The influence of the different input parameters can be interpreted as follows

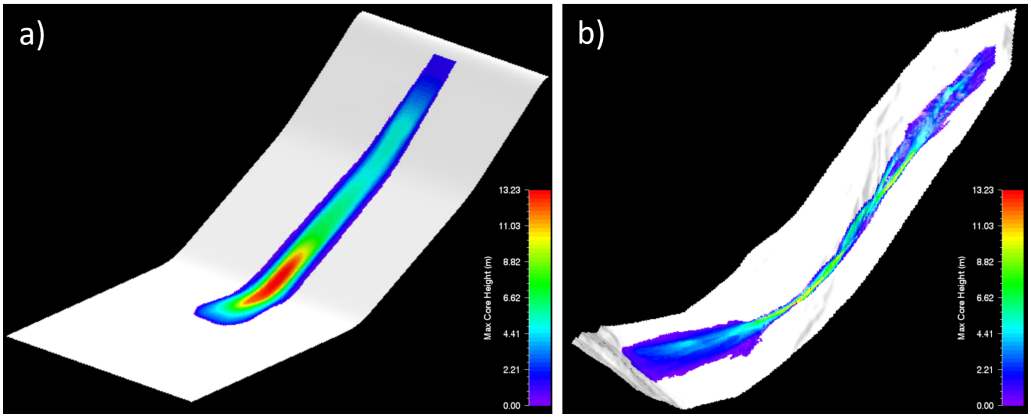

Figure 3: Depiction of the Ruechi Tobel on an a) idealised slope and b) on the summer DEM. Terrain effects turn the avalanche towards the east, see Fig. 2).

with a focus on the core shape:

a) The avalanche length increases with the release depth (i.e. release volume) on both the idealized and real slope. The widths of the core and cloud increase in one direction for the summer DEM simulations as the terrain in the deposition zone is uneven. Additionally, with release volumes exceeding 22'500 m3, flow fingers develop where the avalanche overflows the gully sides. **RAMMS::EXTENDED** has an automatic allocation of the initial friction parameters to a set of predefined volume classes. By varying the release depth, the release volume changes and with this the allocated friction values. This is visible in the diagram as the allocated friction values would change for this example at a release depth below 0.5 m.

b) The influence of erosion depth on avalanche run-out is similar to the release depth. Higher erosion depths leads to longer run-out avalanches as the avalanche size increases. However, unlike the release depth, once the erosion depth reaches a certain value, the run-out length no longer increases, which implies that the entrainment process could dampen avalanche momentum. The entrainment of deep snowcovers requires more energy (more mass must be accelerated), leading to a decrease in avalanche velocity. A balance is struck between the potential energy increase of the entrained snow and the loss of kinetic energy caused by the entrainment. When this balance is reached is determined by a complex interaction of factors, including released and entrained snow volume and temperatures, and terrain.

c) If the erosion gradient is small (small value for ΔD), the erosion height is nearly constant over the entire avalanche track. By increasing the erosion gradient, the erosion height will decrease over the track and less snow can be eroded by the avalanche core. Hence, the avalanche run-out distance and width decreases with increasing erosion gradient as less volume is added to the avalanche from entrainment.

d) Colder temperatures are associated with the formation of fluidized mixed flowing/powder avalanches and generate both longer core and powder cloud run-out distances. This is reflected in the sensitivity model results with colder temperatures generating the longest run-out distances and causing higher powder cloud pressures. This effect is modelled by assuming smaller dissipation rates of fluctuation energy for colder snow granules. The closer the release temperature goes to 0°C, the less fluidized the avalanche, the smaller the avalanche run-out. Of course, if the temperatures are warm enough such that melt-water is created by frictional heating, lubrication effects can occur leading to an increase in avalanche run-out (but not velocity). This did not occur within the range of values tested for in the sensitivity analysis.

e) With a large snow temperature gradient (i.e. larger value for ΔT), the avalanche entrains increasingly warmer snow at lower elevations. This leads to a warmer avalanche core temperature which reduces fluidization in the core. Instead, deposition of the avalanche core is initiated (if the avalanche is not lubricated at this point) resulting in a shorter avalanche run-out distance. The powder cloud also dissipates.

In Figure 5, we investigated how uncertainty in the parameter values related to the practitioner's documentation and knowledge about the snowpack and avalanche details, may influence the modelled avalanche run-out distance and width. To do this, we varied the parameter value using an uncertainty range around the back-calculated parameter values obtained from the Ruechi Tobel avalanche. The interval chosen for the parameter variation depicts the uncertainty related to the practitioner's evaluation. This shows for example for the erosion depth and release depth, that in case the practitioner has a uncertainty of $+/-$ 0.2 m in release depth and $+/-$ 0.1 m in erosion depth, the avalanche length can vary by $+/-$ 75 m for this particular case study.

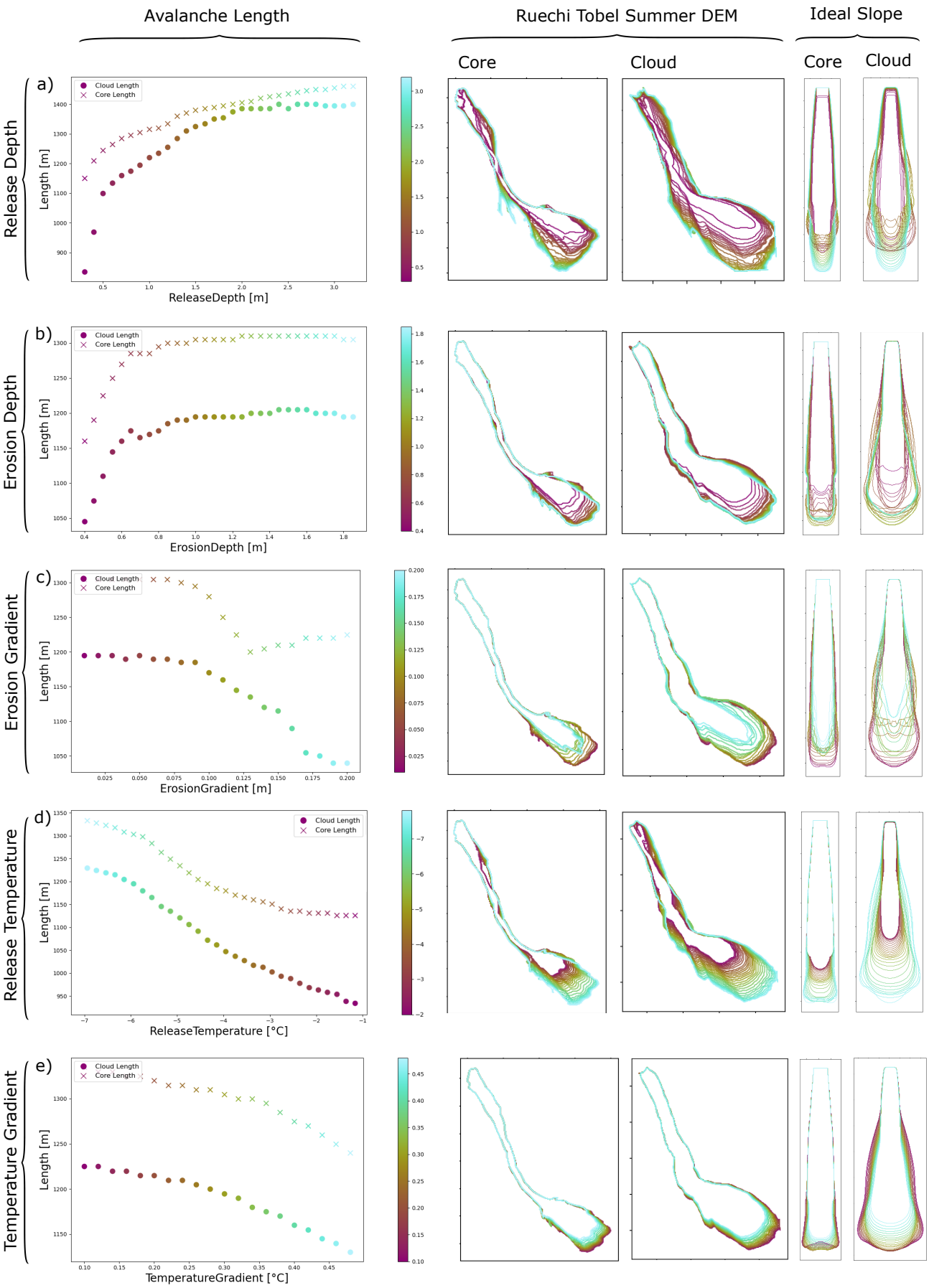

Figure 4: Simulation results for the different input parameters for the Ruechi avalanche on the summer DEM and idealised surface.

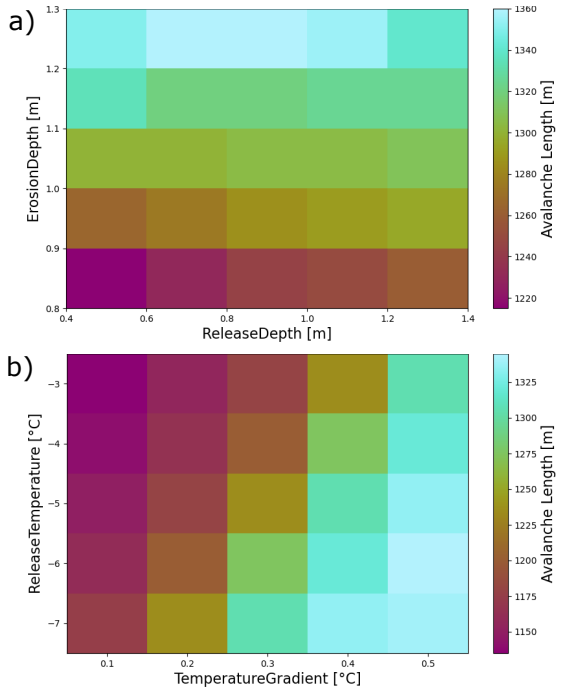

Figure 5: Avalanche length plotted for the variation of a) release depth and erosion depth b) release temperature and the temperature gradient.

4. CONCLUSION AND OUTLOOK

We have extended the **RAMMS::AVALANCHE** model to include temperature effects and the formation and propagation of the avalanche powder cloud. In our sensitivity analysis, we quantified the influence of snow disposition parameters (release depth, erosion depth, snow temperature) on avalanche run-out distance and flow width of both the core and cloud. We evaluated the influence of terrain by simulating avalanches on both an idealized slope and on a real avalanche path. The analysis serves to demonstrate the complex interaction between thermal effects, elevation and terrain and snow disposition on the avalanche flow regime. The release depth and the release temperature show the strongest influence on avalanche run-out distance, independent of terrain, whereas the influence of erosion depth and gradient on avalanche run-out distance and width depend mostly on the terrain. Presently, we have only two temperature dependent parameters (α_Φ, β_Φ) which govern the production and decay of random energy (granular temperature, R_Φ) in the avalanche core. The degree of avalanche fluidization R_Φ, in turn, controls the avalanche flow density and frictional resistance. Here, we state these frictional relationships, with the understanding that much more calibration and validation work remains in the future.

5. ACKNOWLEDGEMENT

This analysis is part of the ”Avalanche Safety for Roads” (Nr. 207519) project founded funded by the Swiss National Science Foundation SNSF.

6. REFERENCES

Bartelt, P., Buser, O., Valero, C., & Bühler, Y. (2015a). Configurational energy and the formation of mixed flowing/powder snow and ice avalanches. *Annals of Glaciology*, *57*, 179–188. https://doi.org/10.3189/2016AoG71A464

Bartelt, P., Christen, M., Bühler, Y., Caviezel, A., & Buser, O. (2018). Snow entrainment: Avalanche interaction with an erodible substrate. *International Snow Science Workshop Proceedings 2018, Innsbruck*, 716–720.

Bartelt, P., Valero, C., Feistl, T., Christen, M., Bühler, Y., & Buser, O. (2015b). Modelling cohesion in snow avalanche flow. *Journal of Glaciology*, *61*, 837–850. https://doi.org/10.3189/2015JoG14J126

Bozhinskiy, A. N., & Losev, K. (1998). *The fundamentals of avalanche science* [ISSN: 0415-0759]. Retrieved August 15, 2023, from https://www.dora.lib4ri.ch/wsl/islandora/object/wsl%3A17257/

Buser, O., & Bartelt, P. (2009). Production and decay of random kinetic energy in granular snow avalanches. *Journal of Glaciology*, *55*. https://doi.org/10.3189/002214309788608859

Christen, M., Kowalski, J., & Bartelt, P. (2010). Ramms: Numerical simulation of dense snow avalanches in three-dimensional terrain. *Cold Regions Science and Technology*, *63*, 1–14. https://doi.org/10.1016/j.coldregions.2010.04.005

Feistl, T. (2015). Forest damage and snow avalanche flow regime. *Natural Hazards and Earth System Sciences*, *15*. https://doi.org/10.5194/nhess-15-1275-2015

Issler, D. (1998). Modelling of snow entrainment and deposition in powder-snow avalanches. *Annals of Glaciology*, *26*, 253–258. https://doi.org/10.3189/1998AoG26-1-253-258

Liu, K., Yin, Z., Chen, W., Weiqiang, F., & Yin, J. (2021). Nonlinear model for the stress-strain-strength behavior of unsaturated granular materials. *International Journal of Geomechanics*, *21*. https://doi.org/10.1061/(ASCE)GM.1943-5622.0002042

Naaim, M., & Gurer, I. (1998). Two-phase numerical model of powder avalanche theory and application. *Natural Hazards*, *17*, 129–145. https://doi.org/10.1023/A:1008002203275

Nazarov, A. N. (1991). Mathematical modeling of a snow-powder avalanche in the framework of the equations of two-layer shallow water. *Fluid Dynamics*, *26*, 70–75.

Ortner, G., Michel, A., Spieler, M., Christen, M., Bühler, Y., Bründl, M., & Bresch, D. (2023). Assessing climate change impacts on snow avalanche hazard. https://doi.org/10.2139/ssrn.4530305

Salm, B., Burkard, A., & Gubler, H. (1990). Calcul des avalanches: Une méthode pour le practicien avec des examples. *IFENA*, *47*.

Saltelli, A., Chan, K., & Scott, E. (2000). *Sensitivity analysis* (Vol. 134).

Turnbull, B., Mcelwaine, J., & Ancey, C. (2007). The kulikovskiy-sveshnikova-beghin model of powder snow avalanches: Development and application. *J. Geophys. Res.*, *112*. https://doi.org/10.1029/2006JF000489

Valero, C., Wever, N., Christen, M., & Bartelt, P. (2017). Modeling the influence of snowcover temperature and water content on wet snow avalanche runout. *Natural Hazards and Earth System Sciences Discussions*, 1–32. https://doi.org/10.5194/nhess-2017-36

Vedrine, L., Li, X., & Gaume, J. (2022). Detrainment and braking of snow avalanches interacting with forests. *Natural Hazards and Earth System Sciences*, *22*, 1015–1028. https://doi.org/10.5194/nhess-22-1015-2022

Voellmy, A. (1955). Über die zerstörungskraft von lawinen. https://doi.org/10.5169/seals-61878

Zhuang, Y., Xing, A., Bartelt, P., Bilal, M., & Ding, Z. (2023). Dynamic response and breakage of trees subject to a landslide-induced air blast. *Natural Hazards and Earth System Sciences*, *23*, 1257–1266. https://doi.org/10.5194/nhess-23-1257-2023